# GLASS MELTING AND ITS INNOVATION POTENTIALS: THE POTENTIAL ROLE OF GLASS FLOW IN THE SAND-DISSOLUTION PROCESS

LUBOMÍR NĚMEC, PETRA CINCIBUSOVÁ

*Laboratory of Inorganic Materials, Joint Workplace of the Institute of Chemical Technology, Prague and Institute of Inorganic Chemistry of the ASCR, v.v.i., Technická 5, 166 28 Prague, Czech Republic*

E-mail: lubomir.nemec@vscht.cz

Submitted February 15, 2009; accepted June 16, 2009

**Keywords:** Sand dissolution, Temperature gradients, Glass flow patterns, Space utilisation, Horizontal channel

*This work demonstrates how the temperature distribution and glass melt flow patterns resulting from these temperature gradients in a simple melting space or tank (horizontal orthogonal channel) influence sand dissolution from the melt, depending on the changes of the utilisation (by changes in the temperature distribution) of the space for the dissolution process occurring along the melt streamlines. The results show that the effect of the glass melt flow pattern and of the consequent space utilisation on the dissolution of the remaining sand are attributable to two quantities, namely the fraction of dead space for the melt flow (the regions in the space with creeping melt flow or the circulation regions of the melt) and the fraction of dead space for the sand particle dissolution (the part of the throughflowing melt where the sand particles are already dissolved). In this work, the volume performance of the space for the bubble removal* $\dot{V}$ *(*$m^3s^{-1}$*) is calculated by using the laboratory value of the sand dissolution time at the average temperature in the melt (1450°C), the mean residence time of glass in the space and the two mentioned quantities characterising the space utilisation. The results are intended to support the control regime for optimising glass melt flow and developing new concepts of industrial dissolution space designs.*

## INTRODUCTION

The requirements of the entire glass-melting process, namely heat, time and space, predetermine two significant criteria of the glass-melting process, i.e. its specific energy consumption and melting performance, which are influenced by the following general factors: temperature, the rate of the homogenisation processes (here the sand-dissolution process), the utilisation of the melting space and the heat flux through the outer boundaries [1–3].

If the specific energy consumption and the volume-melting performance (upon the condition that no inhomogeneities leave the space with the glass melt) are defined for a simple isothermal melting space without energy recirculation [3], the following two equations are obtained:

$$H_M^0 = H_M^T + \frac{\dot{H}^L \tau_H}{\rho V} \frac{1}{u} \ , \qquad (1)$$

$$\dot{V} = \frac{V}{\tau_G} = \frac{V}{\tau_H} u \ , \qquad (2a,b)$$

where $H^0_M$ is the specific energy consumption in $Jkg^{-1}$; $H^T_M$ is the specific theoretical heat necessary for chemical reactions, phase transitions and heating of both batch and melt to the melting temperature $T$ (in $Jkg^{-1}$); $\dot{H}^L$ is the total heat flux across the space boundary in $Js^{-1}$; $\tau_H$ is the reference homogenisation time (here the sand dissolution time obtained by a laboratory crucible melt, for instance) in s; $\rho$ is the glass density in $kg/m^3$; $V$ is the space volume in $m^3$, $\dot{V}$ is the volume flow rate of the melt through the space upon the condition that all the inhomogeneities are removed (here the sand-dissolution performance) in $m^3s^{-1}$; $\tau_G = V/\dot{V}$ is the mean residence time of glass in the space and $u$ is the dimensionless quantity-designating utilisation of the space for the given process, for which it holds that $u \in \langle 0;1 \rangle$ (see below for the definition of quantity $u$ ).

The relevant role of the quantity $u$ ($u \in \langle 0;1 \rangle$), obvious from both equations, is well known to both researchers and technologists, and this quantity is usually interpreted in terms of the mentioned fraction of dead space and the spectrum of melt-residence times in the melting furnace [4]. The high fraction of dead space arises from the circulation regions and regions with creeping flow. The broad spectrum of glass melt residence times in the space is caused by the complex glass flow in the space and results in large quality differences among single homogenisation trajectories. Beerkens claims [5] that the minimum residence time is typically only 15-20% of the average residence time. The mechanism of the sand dissolution process, the existence of dead spaces and differences in the quality

of sand dissolution pathways have been shown by both laboratory studies and mathematical modelling of the process [6-11]. In other words, an important role in performance of the melting process is played not only by the rate of the homogenisation processes but also by the spatial distribution of inhomogeneities.

The aim of this work is to calculate the quantity referred to as the 'utilisation of the space for the sand dissolution process' in the horizontal continuous channel and to study the effect of the glass melt flow pattern caused by the temperature differences on the sand dissolution performance of the space.

## THEORETICAL

The impact of the glass flow patterns in the horizontal continuous glass fining channel on the space utilisation and consequently on the space fining performance was demonstrated in our previous study [3]. The process of dissolution of the remaining sand particles (sand particles present in the melt after the batch reactions have taken place) in most commercial glasses as well as the chemical homogenisation of the melt are processes taking place along the melt streamlines. The volume-dissolution performance of the channel is defined by Equation (2). For the evaluation of the significance of the space utilisation for the sand dissolution process, two component quantities or parameters have been introduced. Both parameters relate to the distribution of undissolved particles in the space and have the form of fractions of dead space. The first fraction of dead space describes the part of the dissolution space where the glass flow is too slow or the melt is circulating, as a result of which no throughflowing melt with particles can enter these regions. The mentioned part of the dissolution space is therefore inefficient for the dissolution process and merges with the dead space for the glass flow

$$m_G = \frac{\tau_G - \bar{\tau}}{\tau_G}; \quad m_G \in \langle 0;1 \rangle , \tag{3}$$

where $\bar{\tau}$ is the average residence time of a melt with particles in the space.

The second fraction of dead space relates to the dissolution quality of individual trajectories. The individual temperature and melt velocity regimes along the streamlines make the individual sand particles dissolve at different distances from the space input, and the points of the complete dissolution of the largest particles create a space function. The point of the complete dissolution of the critical particle just at the output of the space then forms the peak of this function, as it is obvious from Figure 1a,b. At isothermal conditions, the dissolution times of all the particles are identical, hence the critical sand dissolution time, $\tau_{Dcrit}$, is equivalent to the reference dissolution time, $\tau_H$, at the given temperature and the critical trajectory is the fastest one. Non-isothermal conditions make the sand dissolution times on individual trajectories differ, and the shortest time of dissolution does not have to be attained on the critical trajectory (see Figure 1a,b). The minimum particle dissolution time, $\tau_{Dmin} = \tau_H$, is then the base for the calculation of the fraction of dead space for dissolution, $m_D$. The mentioned fraction is described by the following relation

$$m_D = \frac{\bar{\tau} - \tau_{D\min}}{\bar{\tau}}; \quad m_D \in \langle 0;1 \rangle , \tag{4}$$

The quantity $m_D$ can also be interpreted as the measure of the relative width of the residence time distribution function. If $m_D = 0$, a plug flow is set in the space. At isothermal or almost isothermal conditions, $\tau_{Dmin} = \tau_{Dcrit} = \tau_H$.

The space utilisations in Equations (1-2) are then defined by

$$u = (1 - m_G)(1 - m_D); \; u \in \langle 0;1 \rangle \tag{5}$$

The geometrical interpretations of $m_G$ and $m_D$ are obvious from schemes in Figure 1a,b as a part of the space with circulating (or creeping) melt ($m_G$) and the part of the space near the output where the sand particles have already dissolved ($m_D$).

The different temperature distributions in the examined cases with different flow patterns influence the sand dissolution times and as a consequence, also the

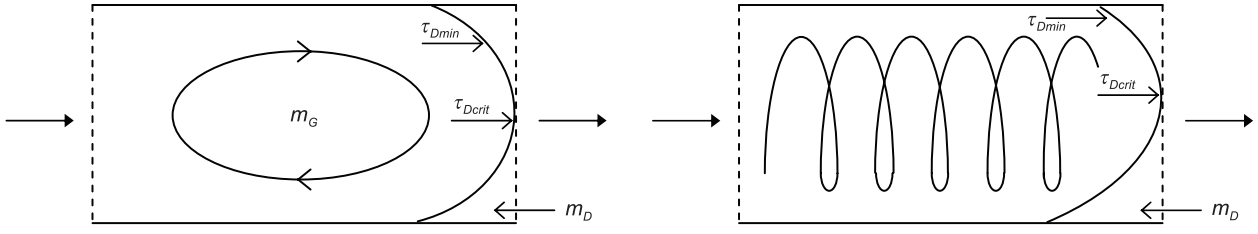


Figure 1. The schematic depiction of the critical and minimum dissolution times of sand particles in the XZ section through the horizontal continuous melting channel. $\tau_{Dmin}$ – the minimum sand dissolution time, $\tau_{Dcrit}$ – the critical sand dissolution time, $m_G$ – the fraction of dead space for the melt flow, $m_D$ – the fraction of dead space for sand dissolution; a) – the channel characterised by the longitudinal circulation flows, b) – the channel characterised by the transversal circulation flows.

values characterising the utilisation of the space. In order to minimise the impact of temperature regimes on the dissolution along individual trajectories, an almost constant overall temperature had to be attained in all the examined cases of this work and the relevant value of the sand dissolution time has been applied.

## CALCULATION CONDITIONS AND RESULTS

The mentioned horizontal channel having a length $l_0$ = 1 m, width $w_0$ = 0.5 m and height of the glass layer $h_0$ = 0.5 m was selected as the model space. The glass melt entered the channel in the YZ front plane of the channel and exited through its YZ back side. As the model glass, the glass for the production of TV panels was applied. Thus, the conditions for calculations were the same as in [3], where the impact of the glass flow pattern on the fining process was examined. The temperature dependence of the glass density and viscosity is described by the following Equations [3]

$$\rho = 2725.1 - 0.238t \; ; \quad (kg/m^3) \quad [t \text{ in } °C]$$
$$\eta = (2.758 \times 10^{-2} - 2.410 \times 10^{-6} t) \exp [6144.6/(t - 437.6)]; \quad (Pas)$$

Appropriate melt flow patterns were formed by applying various temperature boundary conditions (linear temperature gradients). The following temperature boundary conditions have been used: a constant temperature over the channel (isothermal channel), horizontal longitudinal temperature gradients with higher temperatures at the channel input or output, horizontal transversal temperature gradients (the gradients across the channel) and mixed horizontal temperature gradients (both longitudinal and transversal temperature gradients).

The experimentally measured sand-dissolution time at 1450°C was determined to be 1970 s, which corresponded to the value for the same average temperature in [3]. The value has been used in all the calculations as the critical sand-dissolution time. The constant value of the sand-dissolution time applied in the slightly non-isothermal space introduced an error into the calculation of $m_G$ and $m_D$, but this error was reduced by maintaining a constant average temperature in the space. Accordingly, the equality $\tau_{Dmin} = \tau_{Dcrit}$ has been accepted. The results thus demonstrate the pure impact of the glass-flow character on both dead spaces provided that the critical trajectory always has a residence time equal to 1970 s.

The CFD package Glass Service Glass Furnace Model [12] was applied to calculate the temperature and velocity distributions in the horizontal channel (the original form was set out in [12]). Ten thousand massless points were started in the entry profile YZ and traced through the channel. The pull rate of the channel was then being adjusted until the fastest massless point on the critical trajectory left the channel after about 1970 s. This yielded the resulting pull rate and the residence times of the massless points from entrance until their escape from the space.

Figures 2-4 show the horizontal and vertical longitudinal projections of the 25 fastest massless point trajectories in the channels with a longitudinal and reversed longitudinal gradient of 10°C and the trajectories in the channel with a transversal temperature

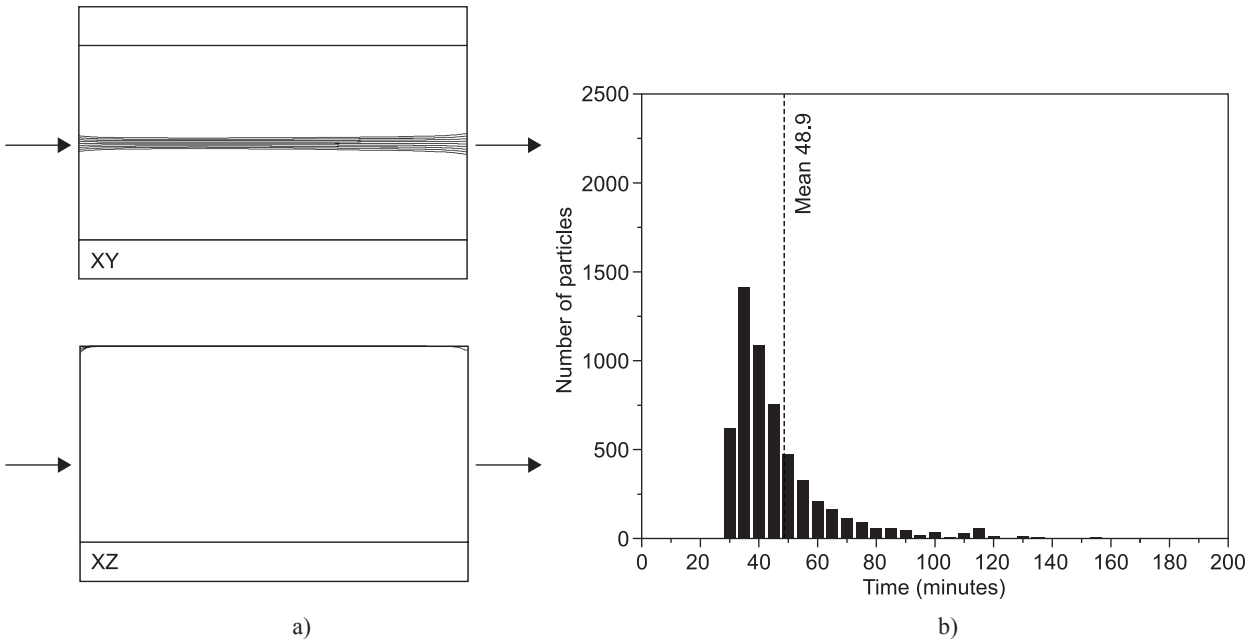


a) b)

Figure 2. The horizontal and vertical longitudinal projections of the 25 fastest massless point trajectories in the channel with the pure longitudinal temperature gradient and the higher temperature at the channel input - ⟨▷10; 0⟩ (a), and the corresponding residence time distribution function (b).

gradient of 25°C/m (a), and the corresponding residence time distribution functions (b). In addition, Figure 5 provides the residence time distribution function for the isothermal channel. The shapes and widths of the residence time distributions in the four cases compared do not show any distinct differences.

Table 1 brings the summarised results of the calculations, i.e. the values of $\dot{V}$, $\bar{\tau}$, $\tau_{Dmin}$, $\tau_G$, $m_G$, $m_D$ and $u$, for individual calculated cases. The calculated cases are labelled by pairs of combined symbols and numbers characterising the type of the longitudinal and transversal linear gradients applied as the boundary conditions for the calculations. The first combination of the symbol and the number has been assigned to the longitudinal temperature gradient and the second one to the transversal temperature gradient. The symbol ▷ denotes the longitudinal temperature gradient with a higher temperature at the channel input and the symbol

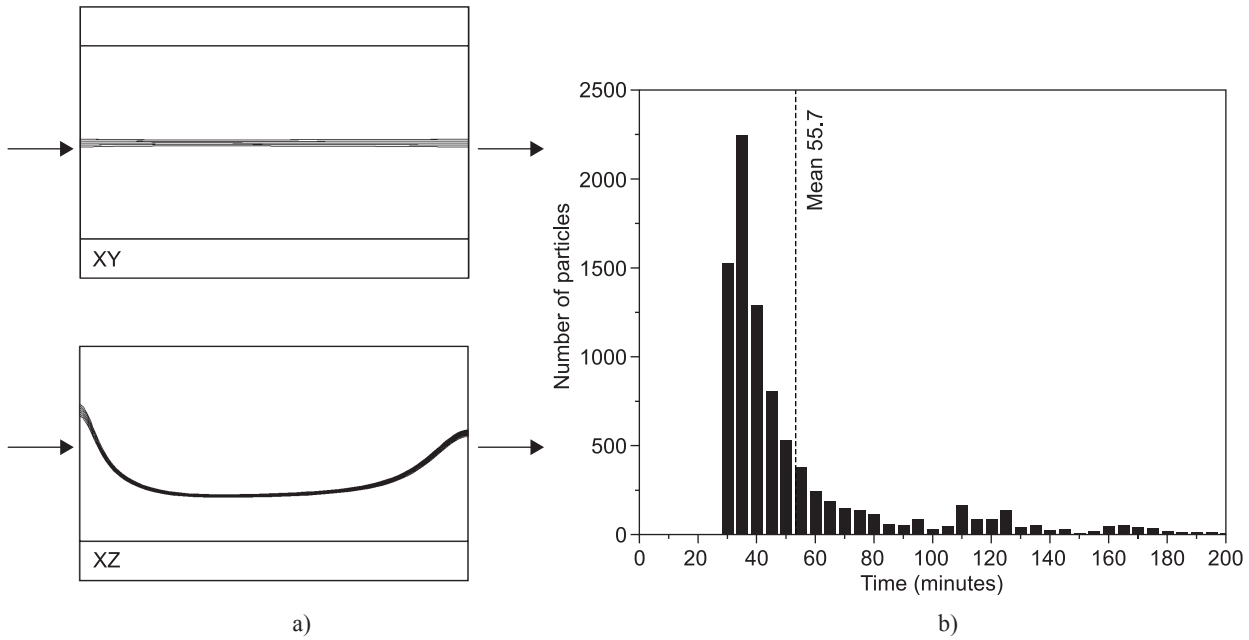


Figure 3. The horizontal and vertical longitudinal projections of the 25 fastest massless point trajectories in the channel with the pure longitudinal temperature gradient and the higher temperature at the channel output - ⟨◁10; 0⟩ (a), and the corresponding residence time distribution function (b).

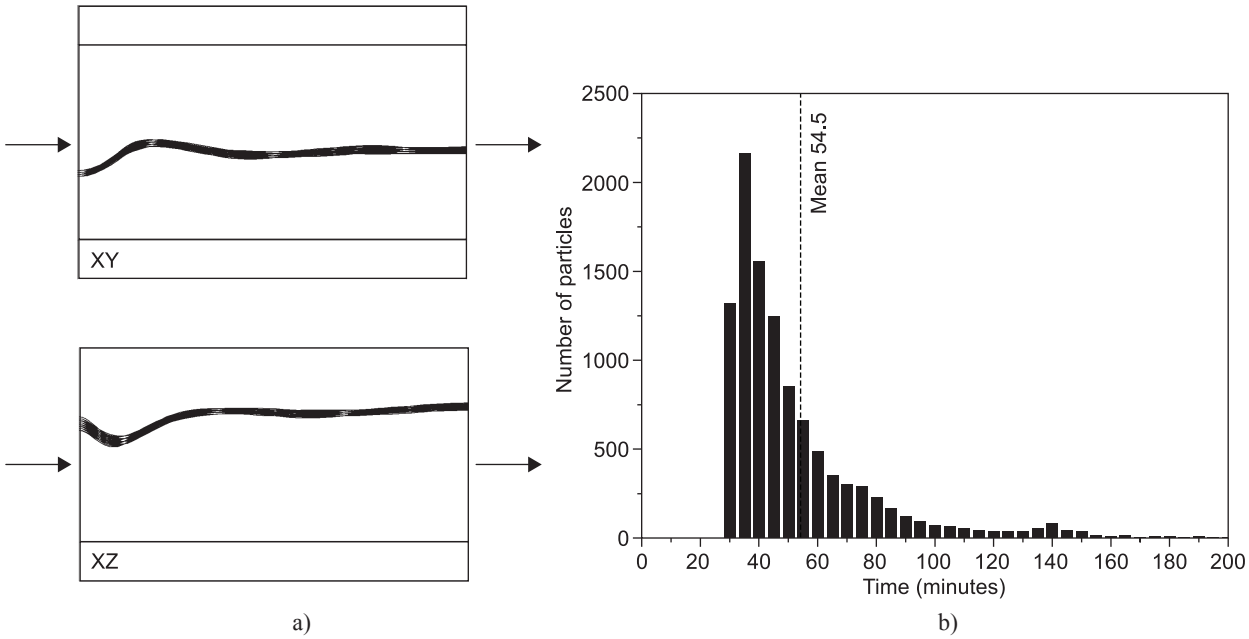


Figure 4. The horizontal and vertical longitudinal projections of the 25 fastest massless point trajectories in the channel with the pure transversal temperature gradient - ⟨0; ↕25⟩ (a), and the corresponding residence time distribution function (b).

◁ the longitudinal temperature gradient with a higher temperature at the channel output, whereas the symbol ↕ designates the transversal temperature gradient and the symbol ↕△ the transversal temperature gradient with the maximum temperature in the centre (a roof shape). The number behind the symbol designates the value of the temperature gradient in °C/m. For example, the pair ⟨▷25; ↕50⟩ refers to the applied longitudinal temperature gradient of 25°C with a higher temperature at the input and the simultaneously applied transversal temperature gradient of 50°C; the pair ⟨◁5; ↕△50⟩ refers to the applied longitudinal temperature gradient of 5°C with a higher temperature at the output and the simultaneously applied transversal temperature gradient of 50°C with a maximum temperature in the centre; the isothermal case is described by the pair ⟨0; 0⟩ etc.

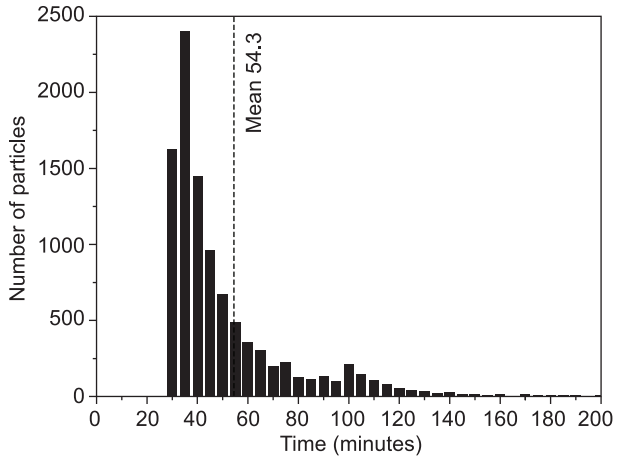


Figure 5. The residence time distribution function of the isothermal channel – ⟨0; 0⟩.

The volume flow rate through the channel approximately characterises the dissolution performance $\dot{V}$ as well as the space utilisation $u$ ( $\dot{V}$ is proportional to the value of $u$, see Equation (2b)) of the channels with different structures of glass patterns (the cases are non-isothermal). In Figure 6, the dependence between $\dot{V}$ and both of the longitudinal temperature gradients has a strictly decreasing character, whereas the value of the dissolution performance in the channel with transversal temperature gradients in Figure 7 is almost independent of the gradient value. High volume flow rates exceeding the volume flow rate of the isothermal channel are apparent in cases described by combinations of a small longitudinal temperature gradient with a higher temperature at the channel output (◁) and a relatively high transversal temperature gradient (see Table 1). The highest values of the volume flow rate (channel dissolution performance), $\dot{V}$ = 8.50×10$^{-4}$ m$^3$/s, have been attained for the cases designated by ⟨◁10; ↕100⟩ and ⟨0; ↕△50⟩. The results show that the maximum channel performance, and hence the space utilisation, is about 67% of the u value, characterising the channel

Table 1. Calculated values: $\dot{V}$ - the volume dissolution performance of the channel, $\tau_{Dmin}$ - the minimum residence time of the melt (the minimum sand dissolution time), $\bar{\tau}$ - the average residence time, $\tau_G$ - the mean residence time ($\tau_G = V/\dot{V}$ ), $m_G$ - the fraction of dead space for glass flow, $m_D$ - the fraction of dead space for sand dissolution, $u$ – the utilisation of the space.

| Temperature boundary conditions (°C/m) | $\dot{V}$ (m$^3$/s) | $\tau_{Dmin}$ (s) | $\bar{\tau}$ (s) | $\tau_G$ (s) | $m_G$ | $m_D$ | $u$ |
|---|---|---|---|---|---|---|---|
| ⟨0; 0⟩ | 7.00E-05 | 1961 | 3258 | 3571 | 0.088 | 0.398 | 0.549 |
| ⟨▷2.5; 0⟩ | 2.63E-05 | 1965 | 3104 | 9524 | 0.674 | 0.367 | 0.206 |
| ⟨▷5; 0⟩ | 1.08E-05 | 1961 | 2936 | 23256 | 0.874 | 0.332 | 0.084 |
| ⟨▷10; 0⟩ | 2.13E-06 | 1957 | 2933 | 117647 | 0.975 | 0.333 | 0.017 |
| ⟨◁10; 0⟩ | 4.06E-05 | 1968 | 3341 | 6154 | 0.457 | 0.411 | 0.320 |
| ⟨◁25; 0⟩ | 2.78E-05 | 1973 | 3361 | 9009 | 0.627 | 0.413 | 0.219 |
| ⟨◁50; 0⟩ | 2.25E-05 | 1961 | 3159 | 11111 | 0.716 | 0.379 | 0.176 |
| ⟨0; ↕5⟩ | 7.38E-05 | 1976 | 3225 | 3390 | 0.049 | 0.387 | 0.583 |
| ⟨0; ↕10⟩ | 7.38E-05 | 1964 | 3240 | 3390 | 0.044 | 0.394 | 0.579 |
| ⟨0; ↕25⟩ | 7.13E-05 | 1961 | 3268 | 3509 | 0.069 | 0.400 | 0.559 |
| ⟨0; ↕50⟩ | 6.75E-05 | 1969 | 3373 | 3704 | 0.089 | 0.416 | 0.532 |
| ↓⟨0; ↕50⟩ | 6.63E-05 | 1975 | 3417 | 3774 | 0.095 | 0.422 | 0.523 |
| ⟨▷5; ↕50⟩ | 5.43E-05 | 1966 | 3905 | 4608 | 0.153 | 0.496 | 0.427 |
| ⟨▷25; ↕50⟩ | 1.63E-05 | 1959 | 14202 | 15361 | 0.075 | 0.862 | 0.128 |
| ⟨◁10; ↕100⟩ | 8.50E-05 | 1966 | 2865 | 2941 | 0.026 | 0.314 | 0.668 |
| ⟨◁6; ↕50⟩ | 8.28E-05 | 1971 | 2958 | 3021 | 0.021 | 0.334 | 0.652 |
| ⟨◁5; ↕25⟩ | 8.26E-05 | 1979 | 2935 | 3026 | 0.030 | 0.326 | 0.654 |
| ⟨◁25; ↕25⟩ | 5.20E-05 | 1966 | 4236 | 4808 | 0.119 | 0.536 | 0.409 |
| ⟨◁2.5; ↕10⟩ | 7.63E-05 | 1972 | 3148 | 3279 | 0.040 | 0.374 | 0.601 |
| ⟨0; ↕△50⟩ | 8.50E-05 | 1961 | 2941 | 2941 | 0.000 | 0.333 | 0.667 |
| ⟨◁5; ↕△50⟩ | 6.75E-05 | 1952 | 3694 | 3704 | 0.003 | 0.472 | 0.527 |

with a plug flow ($\dot{V}$ =1.27×10$^{-4}$ m$^3$/s, $u$ = 1). The values of the volume flow rate and space utilisation should be discussed in terms of the fractions of dead space for the melt flow and sand dissolution, $m_G$ and $m_D$.

## DISCUSSION

The calculated values of $m_G$ and $m_D$ are presented in Table 1. The results comprehensibly explain the dependences between both values and the character of the melt flow caused by the pure (longitudinal and transversal) temperature gradients. The dependences between the values of $m_G$ and $m_D$ and the pure (longitudinal and transversal) temperature gradients are presented in Figures 8 and 9. Both longitudinal temperature gradients (◁ and ▷) in Figure 8 show high values of $m_G$ because of an intensive longitudinal circulation. The $m_G$ values are particularly high for a gradient of the ▷ type ($m_G$ = 0.975 for ⟨▷10; 0⟩), whereas the same values for the longitudinal temperature gradient of the ◁ type are lower when compared with the previous ones, because the longitudinal circulation in the latter case is hindered by the channel bottom. The values of $m_D$ are close to the isothermal case ($m_D$ = 0.398 for ⟨0; 0⟩). The values relate to the distribution of the horizontal velocity of the melt in the active part of the channel space, 1-$m_G$. Nevertheless, the values of $m_D$ for the cases characterised by the symbol ▷ slowly decrease with the growing longitudinal temperature gradient (from 0.398 for ⟨0; 0⟩ to 0.333 for ⟨▷10; 0⟩. The reason for this behaviour is likely to lie in the fact that the space profile of the horizontal velocities becomes flatter (and as a result the residence time distribution function of

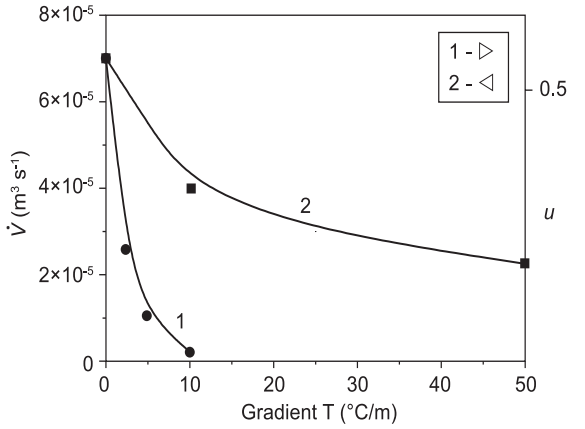


Figure 6. Values of $\dot{V}$ (the volume dissolution performance) as a function of the longitudinal temperature gradient. The cases with longitudinal circulation flows of the glass melt. 1 - the longitudinal temperature gradient of the ▷ type; 2 - the longitudinal temperature gradient of the ◁ type.

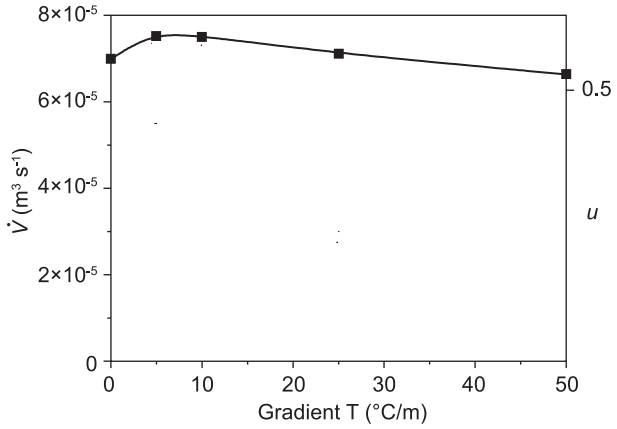


Figure 7. Values of $\dot{V}$ as a function of the transversal temperature gradient. The cases with transversal circulation flows of the glass melt.

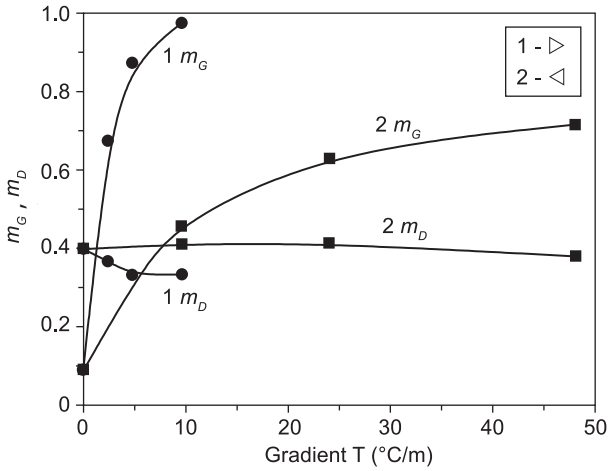


Figure 8. Values of $m_G$ and $m_D$ as a function of the longitudinal temperature gradient. The cases with longitudinal circulation flows of the glass melt; 1 - the longitudinal temperature gradient of the ▷ type; 2 - the longitudinal temperature gradient of the ◁ type.

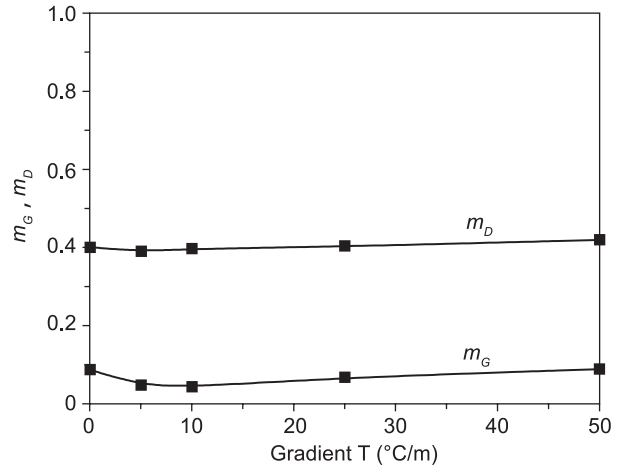


Figure 9. Values of $m_G$ and $m_D$ as a function of the transversal temperature gradient. The cases with transversal circulation flows of the glass melt.

the melt becomes steeper) with a growing temperature gradient of the ▷ type. Summarising the mentioned results, the longitudinal circulation melt flows (the circulation melt flows having the same and opposite directions as the main melt flow through the channel) substantially decrease the active part of the horizontal dissolution space, with the decrease being more distinct for the circulation with the forward flow close to the level, and substantially reduce the dissolution performance of the horizontal melting channel.

The dependences plotted in Figure 9 provide an evidence of the very low value of $m_G$ when the pure transversal circulation melt flows develop in the horizontal channel (the given flow conditions may be theoretically expected to yield the zero value of $m_G$). The values of $m_G$ increase only slightly with the growing transversal temperature gradient (from 0.049 at ⟨0; ↕5⟩ to 0.089 at ⟨0; ↕50⟩), but are generally much smaller when compared to cases with longitudinal circulations. The low value of $m_G$ = 0.094 is kept when the melt inputs the dissolution space through the glass melt level (the input through the glass melt level simulates an industrial melting furnace), the input being characterised by the plane $X \in \langle 0; 0.25\rangle$, $Y \in \langle 0; 0.5\rangle$, and $Z = 0.5$ ($m$), (symbol of the case: ↓0.25 ⟨0; ↕50⟩), and shows a high value of the space utilisation, $u$ = 0.523). Thus, when applying the mentioned circulations perpendicular to the throughflow (working flow) of the melt, the dissolution space is optimally filled up by the continuous spiral trajectories along which the sand particles dissolve and the values of $m_G$ tend towards zero. The values of $m_D$ remain almost independent of the transversal temperature gradient and show approximately the same value as in the isothermal case. The applied simple transversal circulations were therefore unable to make the residence time distribution function steeper and thus to increase the space utilisation and the dissolution performance of the channel due to the decrease in $m_D$ Despite that, the average value of the space utilisation for the cases with transversal circulations, $u$ = 0.555, is substantially higher than the corresponding value for all the longitudinal circulations, $u$ = 0.170. The transversal circulations are therefore much more suitable for the sand dissolution process if the glass melt flows through the space perpendicularly to the established circulations. In addition, the cases with transversal circulations should show higher values of velocity gradients and hence a higher impact of the melt convection on the sand particle dissolution. The relatively high value of the horizontal melt velocity along the critical trajectory in mentioned cases with transversal circulations may be reduced by a convenient modification of transversal circulation, which is why the transversal temperature gradient of the ↕△ type (the roof shape) has been applied. The value of $m_D$

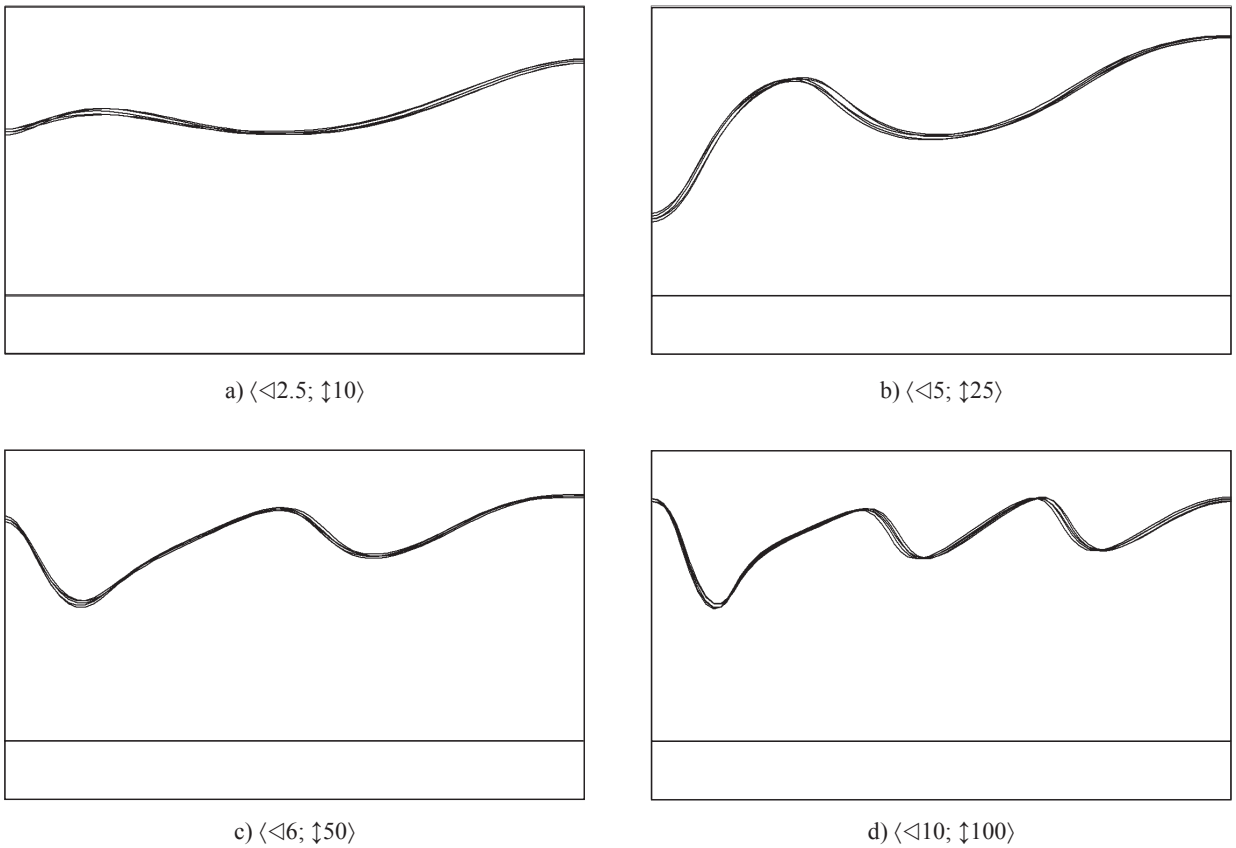

a) ⟨◁2.5; ↕10⟩ b) ⟨◁5; ↕25⟩

c) ⟨◁6; ↕50⟩ d) ⟨◁10; ↕100⟩

Figure 10. The XZ projections of the five fastest melt trajectories in cases characterised by temperature gradients of the ⟨◁$X$; ↕$Y$⟩ type where $Y/X$ is between 4 and 10.

actually decreased to 0.333, and the highest values of space utilisation, $u$ = 0.667, as well as of dissolution performance, $\dot{V}$ = $8.5\times10^{-4}$ $m^3/s$, were attained. The application of proper transversal circulations therefore leads to a slight decrease in the width of the residence time distribution function. Better results might be probably obtained by the application of intensive and irregular transversal flows through the entire cross profile of the space.

The best results as for bubble removal (referred to in [3]) have been obtained in cases combining a longitudinal temperature gradient of the ◁ type and the transversal temperature gradient, with the ratio between them being in the range of 4-10. When considering the possibility of implementing both bubble removal and sand dissolution in the same space, the melt flow character should accommodate both processes. The mentioned combination of the ⟨◁$X$; ↕$Y$⟩ type has therefore been applied in agreement with the results in [3]. These combinations and their results are depicted in Table 1 and show on average the highest values of $u$ and $\dot{V}$ due to the very low values of $m_G$ as well as relatively low values of $m_D$. The values of $m_D$ decreased with the values of both gradients increasing (from $m_D$ = 0.374 at ⟨◁2.5; ↕10⟩ to $m_D$ = 0.314 at ⟨◁10; ↕100⟩), with the value of $m_D$ = 0.314 being the very lowest value of $m_D$. The origin of the low $m_D$ values may be determined from the shapes of the critical trajectories. Figure 10 provides XZ projections of the five fastest trajectories for the four cases studied. Obviously, the number of rotations of the critical trajectory (waves in the projections) increases with the rising values of the temperature gradients, which in fact reduces the average value of the horizontal melt velocity along the pathway. When searching for the critical state ($\tau_{Dcrit}$ = 1970 s), the dissolution performance of the space may therefore be increased. The mentioned combination of the longitudinal and transversal temperature gradients thus keeps the values of $m_G$ low and slightly reduces the width of the residence time distribution function (i.e. $m_D$). The combination of the ⟨◁$X$; ↕$Y$⟩ type – where $Y/X$ was between 4 and 10 - thus appeared favourable for both bubble removal and sand dissolution. Unlike the bubble removal, the good dissolution performance is preserved up to the relatively high values of the longitudinal temperature gradient of the type ◁ . The value of $u$ for the case ⟨◁25; ↕25⟩ is still acceptable, $u$ = 0.409, and the $m_G$ value low, $m_G$ = 0.119, but the value of $m_D$ = 0.536 shows a growth due to a slight broadening of the residence time distribution function.

A comparison of the dissolution performances of the mentioned combinations (combination of the ⟨◁$X$; ↕$Y$⟩ type - where $Y/X$ was between 4 and 10) with the cases characterised by the pure transversal melt flow (the cases ⟨0; ↕$Y$⟩) shows higher dissolution performances of the channels with a small longitudinal temperature gradient of the ◁ type. The slightly lower values of both $m_G$ and $m_D$ in the cases with a longitudinal temperature gradient of the ◁ type are responsible for this behaviour. Figure 11 presents the XZ projections of the five fastest trajectories for the similar cases ⟨0; ↕50⟩ and ⟨◁6; ↕50⟩. The latter case exhibits a more pronounced spiral critical trajectory, which allows a lower value of $\bar{\tau}$, i.e. a higher dissolution performance of the channel. The same, however, does not hold true for comparable cases with a pure transversal temperature gradient of the ↕△ type. Figure 12 compares the five fastest trajectories of the cases ⟨0; ↕△50⟩ and ⟨◁5; ↕△50⟩. Whereas the critical pathway in the former case is partially located in the upper region of the slow forward velocities, the critical trajectory in the latter case is considerably pulled down into the relatively fast forward flow near the bottom. This fact increases the value of  and reduces the dissolution performance of the channel in the case characterised by ⟨◁5; ↕△50⟩.

The results acquired from the calculations of the cases of the ⟨▷$X$; ↕$Y$⟩ type are not easy to interpret. The dissolution performance (and the space utilisation) for the case ⟨▷5; ↕50⟩ decreased from $5.43\times10^{-5}$ $m^3/s$ ($u$ = = 0.427) to only $1.63\times10^{-5}$ $m^3/s$ ($u$ = 0.128) for the case ⟨▷25; ↕50⟩. While the shapes of the fastest trajectories in the case ⟨▷5; ↕50⟩ are very similar to the relative case ⟨0; ↕50⟩ (see Figure 13) and the residence time distribution curves are also similar in both cases, the case with a higher longitudinal temperature gradient, i.e. ⟨▷25; ↕50⟩, shows completely different shapes of the fastest trajectories (see Figure 14a) and also a very different distribution of melt residence times (see Figure 15). The long residence times in the case ⟨▷25; ↕50⟩ are a result of the complicated spiral trajectories of the melt (see Figure 14b), which leads to a substantial broadening of the residence time distribution curve (see Figure 15b), i.e. to a substantial increase in $m_D$. The extension of the residence time distribution function results in a low utilisation of the space and a low dissolution performance. The results show that the cases with comparable longitudinal temperature gradient of the type ▷ and transversal temperature gradient produce flow patterns with oblique spiral trajectories in the channel, have long residence times and are characterised by substantially broadened residence time distribution functions. This implies a low utilisation of the channel space and low dissolution performance of the channel. Similar results have been obtained for the process of bubble removal in the same channel and at the identical temperature [3].

## CONCLUSIONS

The new design of glass melting furnaces requires the conditions of the process to be strictly defined. Besides the temperature or the time-temperature regime, the character of the glass flow in the melting space (both conditions however mutually affect) is one of the principal melting factors. Whereas the melting temperature may easily be predefined on the basis of

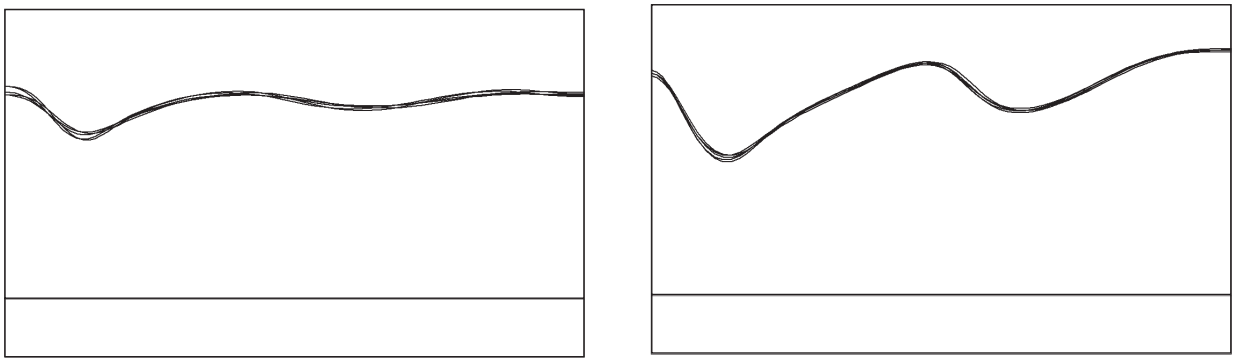

a) b)

Figure 11. The comparison of the XZ projections of the five fastest trajectories for the cases ⟨0; ↕50⟩ (a) and ⟨◁6; ↕50⟩ (b).

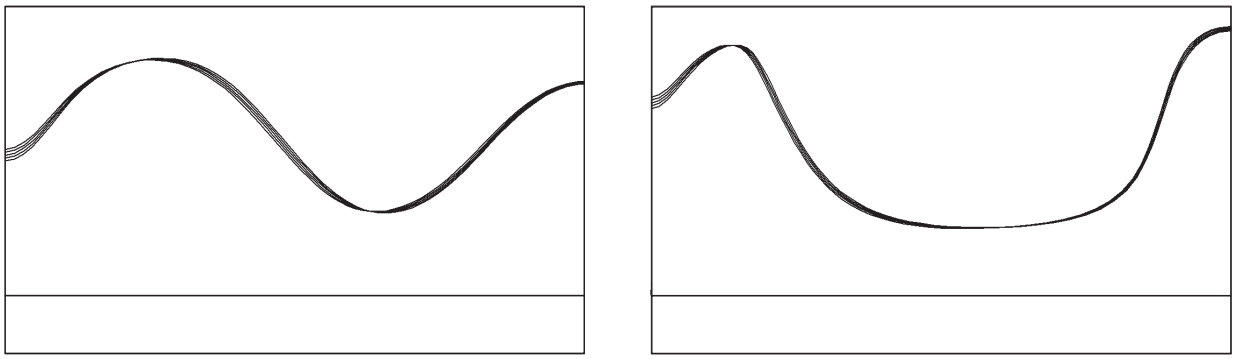

a) b)

Figure 12. The comparison of XZ projections of the five fastest trajectories for the cases ⟨0; ↕△50⟩ (a) and ⟨◁5; ↕△50⟩ (b).

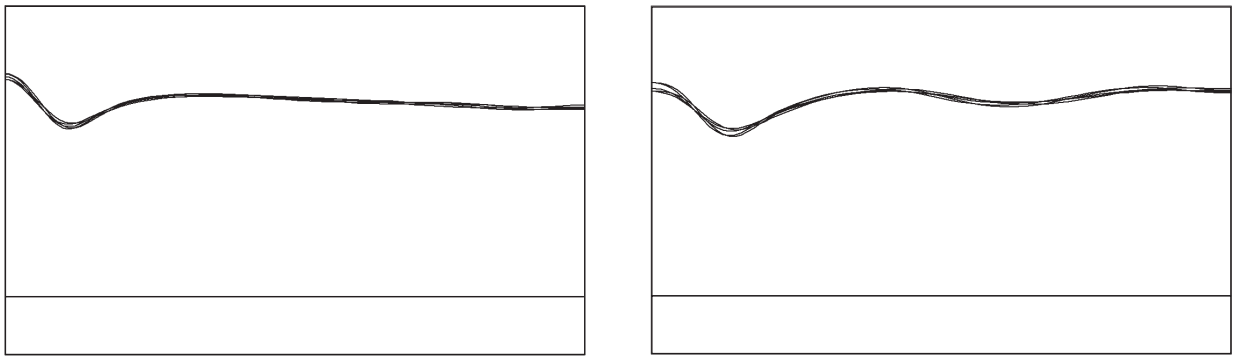

a) b)

Figure 13. The XZ projections of the five fastest trajectories in the cases ⟨▷5; ↕50⟩ (a) and ⟨0; ↕50⟩ (b).

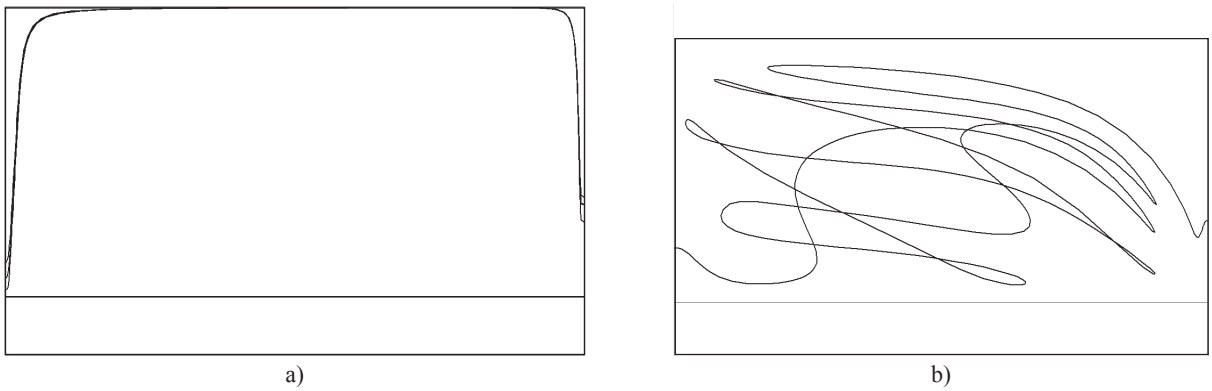

a) b)

Figure 14. The XZ projections of the five fastest pathways (a) and the XY projection of the typical pathway (b) in the case ⟨▷25; ↕50⟩.

laboratory melts, the proper flow character in the melting space, for example, cannot be easily found, particularly due to the absence of clear criteria for an efficient melt flow during the process. The definition of the character of the glass flow by the quantity entitled *utilisation of the space* for the given process provided an opportunity to compare different flow patterns and to define the potentially favourable melt flow structures in the melting space. This work attempted to reveal some characteristics of the different kinds of glass flows, induced by linear temperature gradients in the horizontal melting channel, i.e. under considerably simplified conditions, with the intention of finding their general nature in terms of the sand dissolution process.

The results have shown that the pure longitudinal gradients produced longitudinal circulation glass flows (of the same and opposite directions to the melt throughflow) and resulted in high values of dead space for the glass flow, which reduced the space utilisation for the dissolution process and consequently the space dissolution performance. The pure transversal gradients produced transversal glass flows with spiral glass melt trajectories and showed very low values of dead space for the glass flow (if the melt entered the channel both from the melt level and from the front side) and a residence time distribution of the melt not very different from the cases with longitudinal melt circulations. The utilisation of the space for sand dissolution as well as the space dissolution performance of the cases with only transversal circulations were several times higher when compared to the previous case with only longitudinal circulations. The cases with mixed, approximately identical longitudinal temperature gradients of the type ▷ and transversal temperature gradients exhibited complicated oblique circulation (with respect to the melt throughflow) and approximately spiral melt trajectories, mostly characterised by long and very long residence times. The glass flow patterns were therefore described by the considerably broadened distribution function of the melt residence times, which led to the low utilisation of the melting space, i.e. also to low values of the dissolution performance.

The cases characterised by a relatively high transversal temperature gradient and a small longitudinal temperature gradient with a higher temperature at the output (the ratio between them being in the range of 4-10) hence showed the highest utilisation of the dissolution space and consequently the highest dissolution performance of the channel. Here, the character of the glass flow was similar as in the cases with the pure transversal temperature gradient, but forward motion along the critical trajectories was partially hindered by the effect of the longitudinal temperature gradient. Optimum conditions almost identical with those described before have also been found for the process of bubble removal, described in [3]. This fact is potentially significant for the design of dual-use sand dissolution and bubble removal spaces.

The dissolution efficiency of the space obviously depends on the mutual orientation of the working glass flow (throughflow) and circulation flows in the space, as well as on the mutual driving forces for the transversal and longitudinal circulations. The orientation of the melt working flow perpendicular to the melt circulation planes and the high ratio of the transversal to longitudinal driving forces for circulations in the horizontal space show generally the best results. The high values of the dead space for the glass flow ($m_G$), the broad residence time distribution function (the high values of $m_D$) and consequently the low utilisation of the space ($u$) can always be expected in industrial melting furnaces with the longitudinal circulations being more powerful than the transversal ones. The way to further increase in the utilisation of the special melting spaces probably leads to the application of an intensive mixing perpendicular to the working flow of the melt and with flow patterns showing a very sharp distribution function of the melt residence times.

Acknowledgement

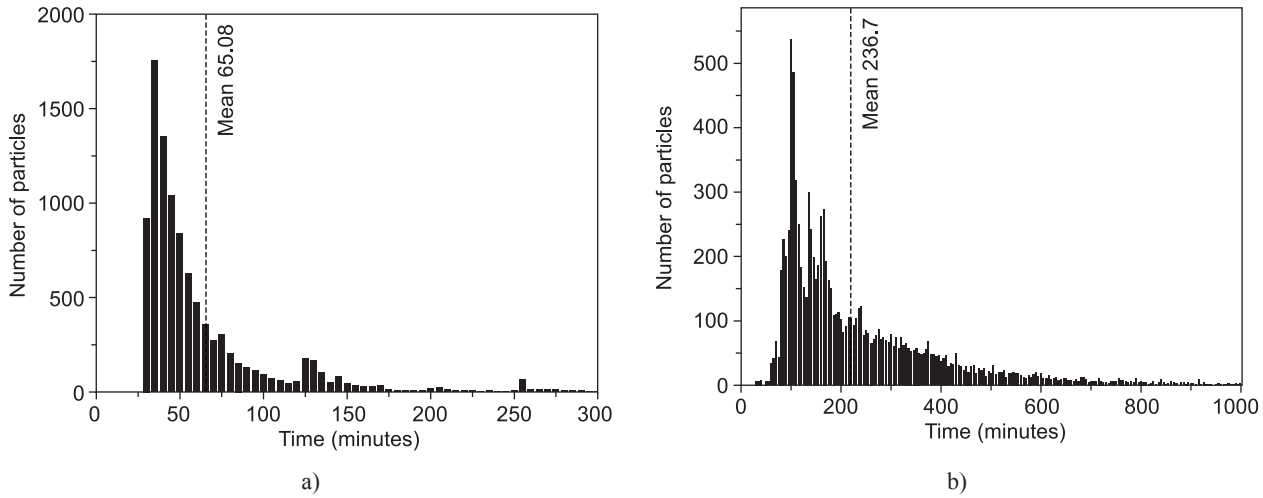


a) b)

Figure 15. The distribution of the melt residence times in the channel for the cases ⟨▷5; ↕50⟩ (a) and ⟨▷25; ↕50⟩ (b).

*This work is part of Project No. 2A-1TP1/063: „New glass and ceramic materials and advanced concepts of their preparation and manufacturing", implemented with the financial support of the Ministry of Industry and Trade and the Institutional Research Plan Proposal No. Z40320502 „Design, synthesis and characterisation of clusters, composites, complexes and other compounds based on inorganic substances; mechanisms and the kinetics of their interactions".*

References

1. Němec L., Jebavá M.: Glass Technol.: Eur. J. Glass Sci. Technol. *A 47*, 68 (2006).
2. Němec L., Jebavá M., Cincibusová P.: Ceramics-Silikáty *50*, 140 (2006).
3. Němec L., Cincibusová P.: Ceramics-Silikáty *52*, 240 (2008).
4. Simonis F., de Waal H., Beerkens R.: Collected Papers XIV. International Congress on Glass, Vol. III, p. 118-127, New Delhi, India 1986.
5. Beerkens R.: Ceramics-Silikáty *52*, 206 (2008).
6. Mühlbauer M., Němec L.: Am. Ceram. Soc. Bull. *64*, 1471 (1985).
7. Němec L., Mühlbauer M.: Glastechn. Ber. *56K*, 82 (1983).
8. Hrma. P., Barton J., Tolt T. L.: J. Non-Crys. Solids *84*, 370 (1986).
9. Bodalbhai L., Hrma P.: Glass technology *27*, 72 (1986).
10. Choudhary M. K.: Glass Technology *29*, 100 (1988).
11. Beerkens R., Muijsenberg E., Heijden T.: Glastechn. Ber. *67*, 179 (1994).
12. Schill P.: Proceedings of the 2nd International Seminar on Mathematical Simulation in the Glass Melting, Vsetín-Horní Bečva, Czech Republic, 17-19 May 1993, pp. 102-116.